https://doi.org/10.5194/egusphere-2024-4188
Preprint. Discussion started: 17 February 2025

Significant Response of Methane in the Upper Troposphere to Subseasonal Variability of the Asian Monsoon Anticyclone

Sihong Zhu[1], Mengchu Tao[1,2*], Zhaonan Cai[1,3], Yi Liu[1,3,4], Liang Feng[5,6], Pubu Sangmu[7], Zhongshui Yu[8], Junji Cao[9]

[1]Carbon Neutrality Research Center, Institute of Atmospheric Physics, Chinese Academy of Sciences, Beijing 100029, China
[2]Key Laboratory for Middle Atmosphere and Global Environment Observation, Institute of Atmospheric Physics, Chinese Academy of Sciences, Beijing 100029, China
[3]Key Laboratory of Atmospheric Environment and Extreme Meteorology, Beijing 100029, China
[4]University of Chinese Academy of Sciences, Beijing 100049, China
[5]National Centre for Earth Observation, University of Edinburgh, Edinburgh, EH9 3FF, UK
[6]School of GeoSciences, University of Edinburgh, Edinburgh EH9 3FF, UK
[7]Linzhi City Meteorological Bureau/CMA Mêdog Field Observatory for Atmospheric Water Cycle, Linzhi, 860000, China
[8]Xizang Institute of Plateau Atmospheric and Environmental Science Research/Xizagê National Climate Observatory, Lhasa, 850001, China
[9]Institute of Atmospheric Physics, Chinese Academy of Sciences, Beijing 100029, China

Correspondence to: Mengchu Tao (mengchutao@mail.iap.ac.cn)

Abstract. Substantial methane (CH_4) emissions in Asia are efficiently transported to the upper troposphere through the monsoon dynamical system, which forms a remarkable seasonal CH_4 enhancement in the upper troposphere. Using a chemical transport model GEOS-Chem driven by surface optimized CH_4 flux, the CH_4 enhancement over the Asian monsoon region is explored as a combined effect of the monsoon dynamical system and regionally increased emissions during late monsoon season. The spatial distributions of CH_4 at the upper troposphere show strong subseasonal variability, which is closely tied to the east-west oscillation of Asian monsoon anticyclone (AMA). Besides, the AMA patterns influence the vertical structure of methane. The AMA center around 80°E favors the upward transport from north India and Bangladesh while the AMA center around 105°E favors the source from southwest China transported to the upper troposphere. The AMA center over the Iranian Plateau suppresses the vertical transport and favors the horizontal redistribution. According to our model sensitivity study, the differences in the upper tropospheric CH_4 anomalies caused by large-scale circulation is 1-2 times of that caused by regional surface emissions. Our research highlights the complex interaction between monsoon dynamics and surface emissions to determine the upper tropospheric methane.

1 Introduction

Methane (CH_4), the second most important greenhouse gas, emitted heavily from south Asia and China, accounts for ~25% of the global anthropogenic emission budget in the recent decades (Stavert et al., 2022). The Asian summer monsoon (ASM) has been proven to be an efficient pathway connecting the rich methane boundary layer and the upper troposphere and lower stratosphere (UTLS) (Randel et al., 2010). The CH_4 enhancement in the upper atmosphere impacts the climate through

https://doi.org/10.5194/egusphere-2024-4188
Preprint. Discussion started: 17 February 2025

radiative forcing (Riese et al., 2012) and influences the stratospheric chemistry, e.g., the methane oxidation (Rohs et al., 2006). More critically, limited understanding of non-local methane sources might mislead the flux inversion from total columns from satellite products (Zeng et al., 2021).

Observations (satellite retrievals and in-situ measurements) and models have evidenced remarkable enhancements of tropospheric tracers over the ASM region in the UTLS, including CO, water vapor, HCN and hydrocarbons, and aerosols (Park et al., 2009; Pan et al., 2016; Randel et al., 2010; Rosenlof et al., 1997; Yu et al., 2017). Similar like other tropospheric tracers, substantial observational evidence showed distinct spatiotemporal distribution of high methane in the middle to upper troposphere over the Asian region during the late monsoon season (Baker et al., 2012; Schuck et al., 2010; Tao et al., 2024; Tomsche et al., 2019) as well as its lasting and traceable pathways into the southern hemisphere and the stratosphere after monsoon withdraw (Belikov et al., 2022; Yan et al., 2019).

The ASM transport structure connecting the surface source regions and the Asian monsoon anticyclone (AMA) in the UTLS has been characteristically described by various studies. The transport system is marked by deep convection, rapidly injecting surface air masses into the UTLS, reaching potential temperature heights around 360 K (~16 km) within hours. Superimposed on the anticyclonic flow, slow diabatic heating with a vertical velocity of about 1–1.5 K/day leads to an upward spiraling movement of air parcels (Bergman et al., 2013; Lau et al., 2018; Pan et al., 2016; Ploeger et al., 2017; Vogel et al., 2019). Significant deep vertical transport is predominantly observed in the southeastern quadrant of the anticyclone, centered near the southern flank of the Tibetan Plateau. This region acts as a 'chimney', where air from the boundary layer is rapidly lifted to the tropopause level, facilitated by vigorous convection over areas like northeast India, Nepal, and the northern Bay of Bengal. The rapid convective uprising process was further characterized by a ‘double-stem-chimney cloud’ (Lau et al., 2018) or ‘two-stem mushroom’ (Pan et al., 2022) structure, which indicates two key areas prominently contributing to the upward transport: the Himalayas-Gangetic Plain and the Sichuan Basin in southwestern China.

One key dynamical feature for the ASM is its subseasonal variability, which is characterized by the active–break cycle of precipitation and surface pressure patterns (Krishnamurti and Ardanuy, 1980; Krishnamurti and Bhalme, 1976), as well as the east-west oscillation of AMA (Nützel et al., 2016; Zhang et al., 2002) with eddy shedding of low potential vorticity (PV) air in the upper troposphere (Garny and Randel, 2013). The variability in the monsoon convection pattern potentially modulates the intensity and position of the AMA (Garny and Randel, 2013; Nützel et al., 2016; Siu and Bowman, 2020). Moreover, the combined effects of convective uplift and anticyclonic confinement jointly shape the distribution and transport of tracers such as CO in the UTLS, as demonstrated and analyzed in previous studies (Luo et al., 2018; Pan et al., 2016).

According to simulations with chemical transport models as well as the satellite observations, the CH_4 enhancement in the upper troposphere (UT) over Asian monsoon region varies from 3% to 10% (Park et al., 2004; Tao et al., 2024; Xiong et al., 2009). The relevant studies rarely use CH_4 as monsoon transport tracer due to its complicated emission sources. Different from tracer like CO, that has primarily industrial sources and hence displays little seasonal variation, CH_4 emissions in Asia,

https://doi.org/10.5194/egusphere-2024-4188
Preprint. Discussion started: 17 February 2025

predominantly (over 60%) from rice cultivation (Stavert et al., 2022), exhibit significant seasonality. The debate persists over whether the seasonal increase of UT methane in the Asian monsoon region is due to enhanced summer emissions from regional rice paddies (Zhang et al., 2020) or the upward transport by the monsoonal circulation (Zeng et al., 2021). Hence, it is crucial to understand how the lower boundary methane conditions and monsoon circulation interact with each other.

The purpose of this study is (1) to explore the association of UT methane over ASM with subseasonal variability of AMA dynamics and (2) quantify the relative role of the AMA dynamics and regional emissions in shaping UT methane. The state-of-the-art approach for the goal is model simulations with a data assimilation system. The reasonable representation of UT CH_4 over ASM with this model has been proven through a comprehensive comparison with satellite and in-situ observations in a previous study (Tao et al., 2024). In this study, we first show the subseasonal behaviour of UT methane modulated by the AMA using the case of summer 2020. Then, we analyze the methane transport pathways under different AMA modes through mode composites. Lastly, we examine the UT methane change in association with AMA dynamics and surface emission respectively, through a model sensitivity study.

2 Data and Method

2.1 Global 3-D methane simulation

We use v12.5.0 of GEOS-Chem (http://www.geos-chem.org, The International GEOS-Chem User Community, 2019) to generate of global 3-D methane concentrations for the period 2015–2020, with a temporal resolution of 1 day and a spatial resolution of $2^{\circ} \times 2.5^{\circ}$ (longitude × latitude). The model is driven by the Modern-Era Retrospective Analysis for Research and Applications version 2 (MERRA-2) re-analysis from the Global Modelling and Assimilation Office of NASA (Gelaro et al., 2017). For consistency, we also use MERRA-2 reanalysis data to analyze dynamical fields.

The surface CH_4 fluxes used in the transport model are optimized with atmospheric observations via an ensemble Kalman Filter (EnKF) framework (Feng et al., 2009, 2017). In the framework, the *a priori* emission estimates include natural sources (e.g., wetlands, fires, termites), and anthropogenic sources (e.g., fossil fuels, livestock, rice, and waste) as detailed in Zhu et al., (2022). The atmospheric CH_4 observations include the proxy GOSAT v9.0 column methane data (XCH_4) from the University of Leicester (https://catalogue.ceda.ac.uk/uuid/18ef8247f52a4cb6a14013f8235cc1eb, Parker et al., 2020) and near-surface methane mole fraction samples from the CH_4 GLOBALVIEWplus v5.0 ObsPack (https://gml.noaa.gov/ccgg/obspack/release_notes.html#obspack_ch4_1_GLOBALVIEWplus_v5.0_2022-10-17, Schuldt et al., 2022).

The inverted flux-driven global 3-D methane concentrations were evaluated using observations from several platforms, including ground-based XCH_4 measurements from the Total Carbon Column Observing Network (TCCON) (https://tccondata.org/, TCCON Team, 2022), CH_4 flask samples collected by aircraft in the Comprehensive Observation Network for TRace gases by AIrLiner (CONTRAIL) project (https://www.cger.nies.go.jp/contrail/index.html, Machida et al.,

https://doi.org/10.5194/egusphere-2024-4188
Preprint. Discussion started: 17 February 2025

2023) and CH_4 profiles from ground to 25 km measured over the Tibetan Plateau by an AirCore air sampling and data processing system (Tao et al., 2024). In our simulation experiments, only surface CH_4 flux is varied, with no alterations to meteorological fields or initial conditions.

2.2 Classification of Asia monsoon anticyclone modes

In a series of previous studies, the subseasonal variability of AMA has been characterized as 'bimodality', referring to two major modes: Tibetan mode and Iranian mode (Nützel et al., 2016; Zhang et al., 2002). However, the existence and nature of this bimodality remain a topic of ongoing debate, with some study arguing that the bimodality is not a prominent feature for the AMA climatological state (Manney et al., 2021). It is important to note that our study does not aim to confirm the existence of AMA bimodality or to explore its underlying dynamics. We aim to investigate the relationship between AMA subseasonal variability and the three-dimensional distribution and transport of methane.

Following the methodology outlined in Zhang et al. (2002), the AMA centers are identified as the positions of geopotential height (GPH) peaks along the ridgeline of anticyclone (zero u-wind within the ASM region (30°W-180°E, 10°N-40°N)) using wind and GPH from MERRA-2 reanalysis. We exclude centers with GPH values in the lowest 70% of the GPH range measured along the ridgeline. Different from previous studies that commonly use 100 hPa as a reference, we use the 150 hPa pressure level because both convection-driven vertical uplift and horizontal confinement are active at this layer, providing significant variability in AMA and its impact on tracer transport. Meanwhile, the anticyclonic circulation basically remains closed at 150 hPa.

The probability distribution of AMA center positions in our study exhibits a pattern resembling bimodality, though it is less distinct than that reported in Zhang et al. (2002). Our statistics show that the frequency of the Tibetan mode (the eastern phase of the distribution) is nearly twice that of the Iranian mode. Additionally, we observe a less pronounced bimodal feature within Tibetan Plateau (TP) cases, prompting us to further subdivide the Tibetan mode into the East Tibetan Plateau mode and the West Tibetan Plateau mode, based on the AMA's position relative to the longitudinal meridian of ~90°E (the center of heating in the TP). Previous study has also noted the different effects of the AMA being centered on the east or west side of the Tibetan mode on upper tropospheric tracers and thus introduced more classification (Tomsche et al., 2019). This classification also aligns with our subsequent analysis of the corresponding source regions.

The AMA modes are therefore classified according to the number and position of AMA center(s) on a daily basis for six boreal summers (July, August and September, JAS) from 2015 to 2020. Dates with a single center are categorized by the longitudinal position of the center: 40-70°E defining as the Iranian Plateau (IP) mode, 75-90°E as West Tibetan Plateau (WTP) mode, and 95-120°E as East Tibetan Plateau (ETP) mode.

https://doi.org/10.5194/egusphere-2024-4188
Preprint. Discussion started: 17 February 2025

3 Results

3.1 Subseasonal variability in upper tropospheric CH_4 during 2020 Asian summer monsoon

We firstly examine the influence of the ASM on the vertical distribution of CH_4 in 2020 summer. Hovemoller diagram shows the anomalies of GPH as well as methane on 150 hPa refer to their daily means over the main ASM region (15°N-40°N, 15°E-135°E; Figure 1). The AMA experienced 4 east-west oscillations from July to mid-August (Figure 1a), commencing with a positive GPH anomaly around 85°E-90°E —attributable to thermal heating in the TP—followed by a westward migration due to instability. From mid-August, the AMA center over predominantly hovered east of 75°E. These subseasonal variability of AMA has a pronounced influence on the distribution of CH_4 in the middle to upper troposphere (see Figure 1b). Simulated CH_4 is highly correlated (r = 0.78) with the geopotential height field.

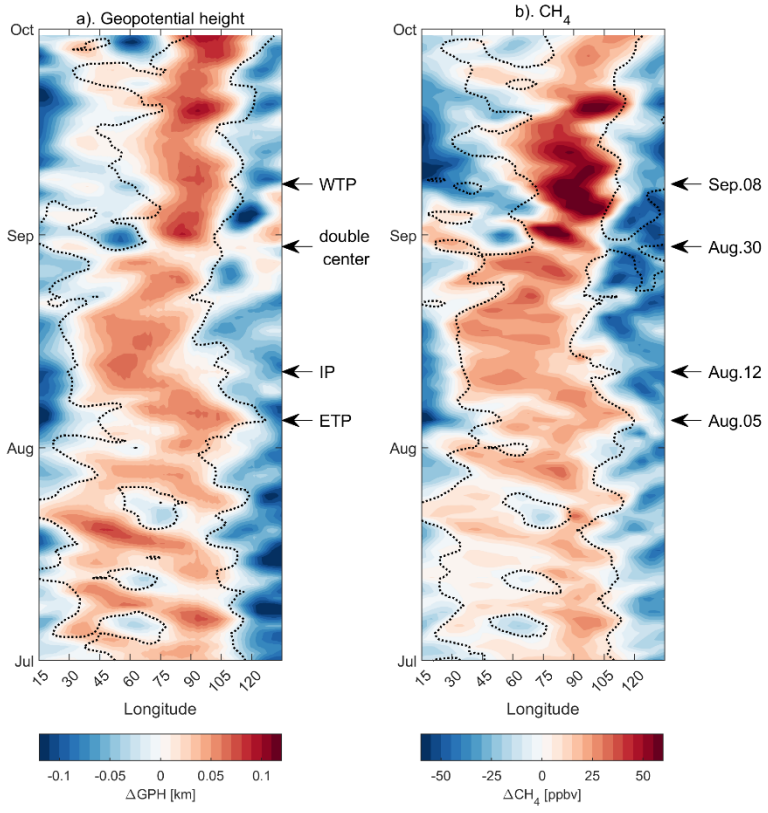

Figure 1: Hovemoller diagram of geopotential height (a) and CH_4 (b) anomalies at 150hPa for JAS 2020. The anomalies refer to the daily means over the main ASM region (15°N-40°N, 15°E-135°E). The zero contour (dotted line) is plotted on opposite filed. The Pearson's Correlation coefficient between the two fields is 0.78.

The east-west migration of CH_4 anomalies mirrors the subseasonal oscillations of the AMA, revealing the dynamic nature of methane distribution over monsoon region. Hereby we select 4 days to illustrate the spatial distribution of methane and dynamical fields under typical AMA modes in Figure 2: East Tibetan Plateau (ETP) mode centering 90°E-110°E (Aug. 5th),

https://doi.org/10.5194/egusphere-2024-4188
Preprint. Discussion started: 17 February 2025

Iranian Plateau (IP) mode centering 50°E-60°E (Aug. 12th), double center mode (Aug. 30th) and West Tibetan Plateau (WTP) mode centering 80°E-90°E (Sep. 8th). The daily maps show that although the CH_4 enhancement was largely confined within AMA, CH_4 peak does not invariably align with the AMA center. For example, at IP mode on Aug. 12st (see Figure 2b), the high methane center locates southern edge of AMA, which results from "stirring" interaction between uplifted boundary layer air and surrounding air.

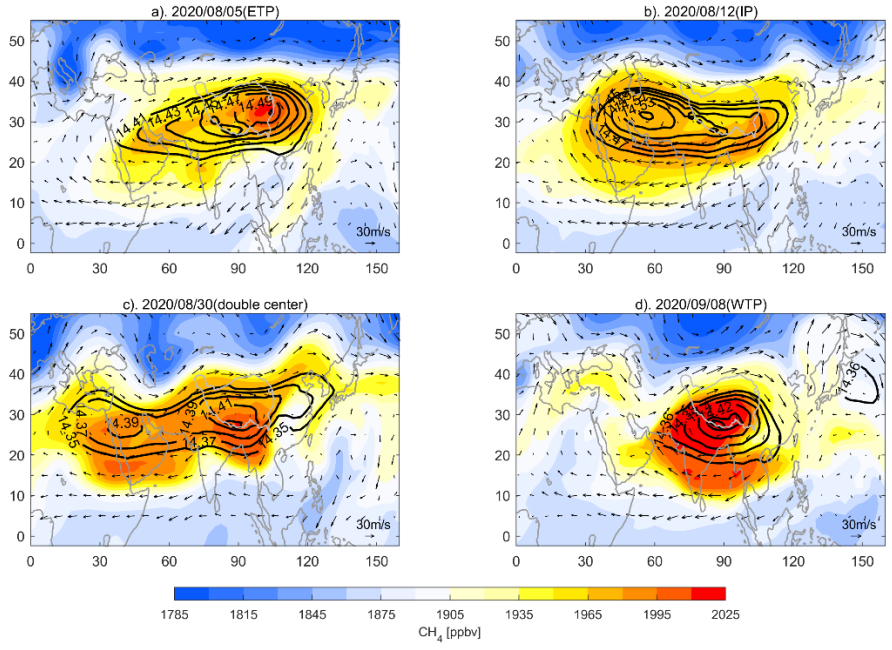

Figure 2: Map of daily mean methane on 150hPa (color shades) for four selected days (arrows in Figure 1), as examples for the methane behavior under different phases of AMA oscillation. The black lines show the AMA center (select GPH contours) and the vectors indicates the wind on 150hPa.

The subseasonal dynamical control of AMA on CH_4 in the middle to upper troposphere is similar as other tracer like CO (Luo et al., 2018; Pan et al., 2016). Contrasting with CO—which typically shows a significant increase in UT around mid-June, correlating with the onset of the South Asian monsoon and its associated convective transport—we observe a pronounced increase in CH_4 concentrations at UT in mid-August, e.g. notably CH_4 increase within the 75°E-110°E longitudinal range in Figure.1. The timing of this CH_4 surge aligns closely with the seasonal emissions peak from rice paddy cultivation.

Observed the methane behavior throughout this summer, the monsoon large-scale circulation dynamics with a strong subseasonal variability clearly manipulate the spatial distribution of upper tropospheric CH_4, which is similar as tracers like CO and water vapor. Meanwhile, the temporal subseasonal variation of the mean CH_4 concentrations over AMA (a remarkable integral rise during mid-August and September) potentially relates to increased emissions in late monsoon season.

https://doi.org/10.5194/egusphere-2024-4188
Preprint. Discussion started: 17 February 2025

3.2 Composites of AMA modes

To extend the 2020 summer case to a general picture of CH_4 distribution under different AMA status, we composite the methane daily fields for 6 summers (JAS during 2015-2020) according to the corresponding AMA modes (see the Method section for the classification). Figure 3 presents the vertical structure of methane (longitude-pressure cross section) associated with three single-center modes (WTP, ETP and IP mode). It reveals that high concentrations of methane in the boundary layer are localized between 60°E to 105°E and undergo a redistribution to a broader area in the upper troposphere (300-100hPa).

This distribution emerged with the "double-stem-chimney cloud" or "two-stem-mushroom" structure, as characterized by (Lau et al., 2018; Pan et al., 2022), i.e., the two narrow "stems" (centered on 80°E and 105°E, respectively) indicating vertical pumping by deep convections as well as the "cap" resulting from the expanding the uplifted near-surface air masses through quasi-isentropically transport. The composites add details to the "two-stem-mushroom" structure. The WTP mode favors the vertical uplifting over 80°-90°E (western "stem") while the ETP mode favors the vertical transport over 100°-110°E (eastern "stem"). Under IP mode, the horizonal redistribution is remarkable with a weak vertical pathway. Previous study has identified two key regions in connection with these two transport "stems": one is the Himalayas-Gangetic Plain mainly including the northern Indian region and Bangladesh, and another one is southwest China (Lau et al., 2018, see also the surface flux map for monsoon season in Figure.S1).

https://doi.org/10.5194/egusphere-2024-4188
Preprint. Discussion started: 17 February 2025

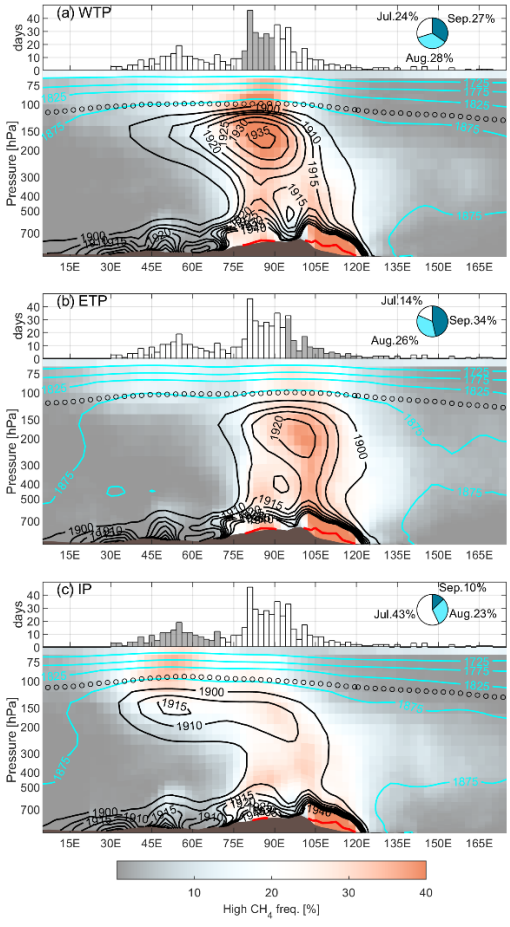

Figure 3: Composites of the longitude-pressure cross section of methane (averaged over 15°N-40°N) for the three modes (2015-2020 JAS). The contours show the averaged methane volume mixing ratios (VMRs) for each mode (VMRs less than 1900ppbv shown as cyan contours and VMRs equal or greater than 1900ppbv shown as black contours). The color shades indicate the occurrence frequency (unit: %) of high CH_4 VMR (criteria: higher than 90% of grids within the Asian monsoon region on the same model level). The longitude distribution of GPH maximum along the anticyclone ridge is plotted on the top of each panel, where the grey bars cover the longitude range for corresponding mode. The pie charts show the proportions of months for each mode.

Figure 4 further shows horizonal view for the conjunction of source regions with CH_4 enhancement in the UT. The current findings suggest that the WTP mode facilitates the first pathway to the UT (see Figure 4 left column, a1-a3), whereas the ETP mode is more conducive to promoting the second pathway (Figure 4 middle column, b1-b3). The IP mode composite (Figure 4 right column, c1-c3) demonstrates that while UT methane enhancement is observed between 45°E to 60°E, the corresponding enhancement at the boundary layer is located similarly to the TP modes—specifically, at the southern edge of the Tibetan Plateau. This suggests that the UT enhancement during the IP mode is not primarily a result of direct vertical pumping but rather a complex redistribution involving the boundary layer air within the ambit of the AMA.

https://doi.org/10.5194/egusphere-2024-4188
Preprint. Discussion started: 17 February 2025

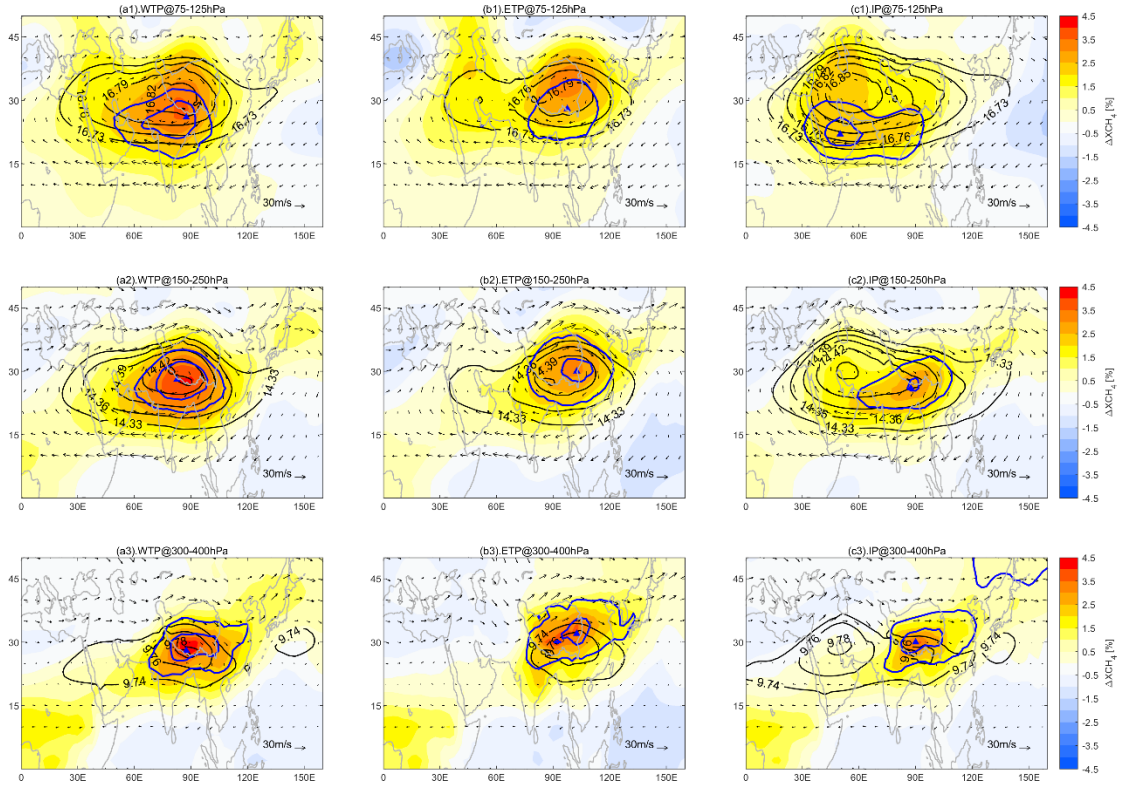

Figure 4: Horizonal distribution of the 3 mode composites at the middle troposphere (300-400hPa, bottom panels a3-c3), the upper troposphere (150-250hPa, middle panels a2-c2) and the lowermost stratosphere (75-125hPa, top panels a1-c1). The color shades show the XCH4 anomalies (unit: %, referring to zonal mean) within the concern pressure range. The black contours indicate the AMA (GPH contours). The blue lines mark the region with high occurrence frequency (50% and 70% are plotted) of elevated methane (definition same as Figure 3) and the triangles mark the location with highest occurrence frequency.

Among the three composites, it is evident that the WTP mode offers the most effective transport pathway for rich methane air from Himalayas-Gangetic Plain to the UT. The methane enhancement observed in the UT during the WTP mode is nearly twice (4~5%) that observed in the IP mode (~2%) and also stronger than ETP mode (~3%). According to the limited statistical samples, we also found that IP mode predominantly manifests during Julys, while the ETP mode is more frequently observed in Septembers. This phenomenon is also observed in the 2020 case as shown in Figure 1.

3.3 Contribution from the emissions and dynamics of ASM system

In Sections 3.1 and 3.2, we demonstrate that variability in UTLS methane over the Asian region is influenced by two main factors: firstly, the dynamical east-west oscillation of the ASM, which substantially modulates methane distribution and influence the upward transport pathways; secondly, the increase in methane emissions from rice paddy cultivation in late August and early September, which potentially intensify the upper-level methane structure during the late monsoon season.

https://doi.org/10.5194/egusphere-2024-4188
Preprint. Discussion started: 17 February 2025

In this section, we further quantify the contributions of these two factors—specifically, surface emissions and ASM dynamics—to regional methane enhancement, allowing us to assess their relative impact on methane variability in the UTLS.

Figure 5(a) presents the time series of total methane emissions (blue line) and methane concentrations in the UTLS (orange line), averaged over the Asian summer monsoon (ASM) region (15–40°N, 15–135°E). The results indicate that the annual maxima of UTLS methane concentrations generally coincide with the peaks in annual emissions. Furthermore, years with higher late-summer emissions tend to correspond to elevated methane concentrations in the UTLS. For instance, during JAS (July–September) 2020, when seasonal emissions reached a relatively high value (~19.3 Tg for the entire ASM region), the UTLS methane concentration also peaked (~1928 ppbv), marking the maximum throughout the simulation period.

Meanwhile, we notice that the interannual variability of methane in the UTLS (orange line) during the monsoon season is 40% larger than other seasons, while the emissions during monsoon did not show remarkably larger interannual variability than other seasons. This suggests that upper level methane during monsoon season are not solely determined by emission magnitude but to some extend influenced by the ASM dynamical conditions. For example, while the seasonal total emissions during JAS 2016 and 2018 are comparable (18.3 Tg versus 18.4 Tg), the methane concentration in the UTLS during JAS 2018 is ~30 ppbv (~1.5%) higher than in 2016, which is a remarkable interannual difference. This difference can be attributed to variations in the distribution of anticyclone modes (Figure 5b & Figure S2). Specifically, during JAS 2018, the ASM anticyclone exhibited a higher frequency of WTP (western Tibetan Plateau) and ETP (eastern Tibetan Plateau) modes, particularly in August and September, creating a more favorable configuration for upward transport compared to 2016. A detailed comparison of subseasonal oscillations of the AMA between 2016 and 2018 is provided in the supplementary material (Figure S2).

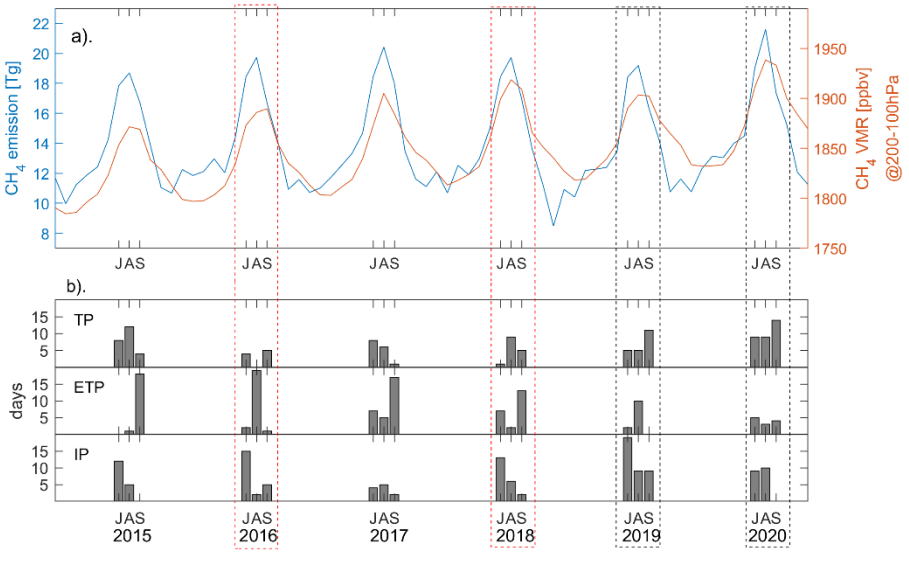

Figure 5: a) Time series of monthly methane total emission (unit: Tg) and VMRs (unit: ppbv) averaged over ASM region (15-40N, 15-135E). (b) The number of days identified for three modes during July, August and September for each year.

https://doi.org/10.5194/egusphere-2024-4188
Preprint. Discussion started: 17 February 2025

Based on the analysis above, we assess the relative contribution of emissions in the lower boundary and AMA dynamics to the upper level methane through a sensitivity test. We use the AMA dynamics of 2016 and 2018 as representative cases to examine configurations that suppress or enhance UTLS transport, respectively. To isolate the impact of AMA configuration, we conducted a test simulation using the lower boundary emissions of 2016 combined with the meteorological data of 2018 to drive the model (16LB/18Dyn). The resulting change in methane concentrations, compared to the control run for 2016 (16Ctl), represents the effect of AMA dynamics. To confirm that these results are independent of the boundary conditions, we conducted a parallel test using the lower boundary emissions of 2018 combined with the meteorological data of 2016 (18LB/16Dyn). The methane changes were then compared to the control run for 2018 (18Ctl). We found that the results of 16LB/18Dyn-16Ctl and 18Ctl-18LB/16Dyn were nearly identical (see Table 1 and Figure S3). Consequently, we use the 16LB/18Dyn - 16Ctl simulation to illustrate the influence of AMA dynamics in the following analysis.

Table 1. Seasonal (JAS) and ASM regional (15-40N, 15-135E) mean CH4 VMR (unit: ppbv) in the UTLS (200-100hPa) for the control and test runs.

	Control run		Test runs		Diff. (test-control)
Fixed L.B.	16Ctl	1883	16LB/18Dyn	1903	20 (1.06%)
	18Ctl	1909	18LB/16Dyn	1888	-21 (-1.11%)
Fixed Dyn.	19Ctl	1899	20LB/19Dyn	1912	13 (0.68%)
	20Ctl	1928	19LB/20Dyn	1912	-16 (-0.83%)

Additionally, we use the lower boundary conditions of 2019 and 2020 as representative cases for low and high emissions over the ASM region, respectively. The total emissions over the ASM region during JAS 2020 are remarkably higher (1.3 Tg, ~7%) than those in 2019. To isolate the effect of emissions, we conducted a test simulation using the lower boundary emissions of 2020 with the meteorological data of 2019 (20LB/19Dyn) and compared the results to the control run for 2019. Similarly, we ran a test replacing the 2020 lower boundary with the 2019 emissions (19LB/20Dyn). We found that the differences due to variations in the lower boundary emissions remained relatively consistent when using different dynamical fields (see details in Figure S4). Therefore, in the following analysis, we use the results from 20LB/19Dyn-19Ctl to illustrate the effect of surface emissions.

Figures 6 and 7 illustrate the spatial distribution of the effects from monsoon dynamics and emission conditions, respectively. Quantitatively, monsoon dynamics introduce stronger variations in methane concentrations (1–2%) in the UTLS region compared to the changes driven by emissions, which are less than 1%. This difference arises because the impact of dynamics is amplified in the UTLS region (Figure 6a), while the influence of emissions diminishes progressively from the surface to higher altitudes (Figure 7a).

https://doi.org/10.5194/egusphere-2024-4188
Preprint. Discussion started: 17 February 2025

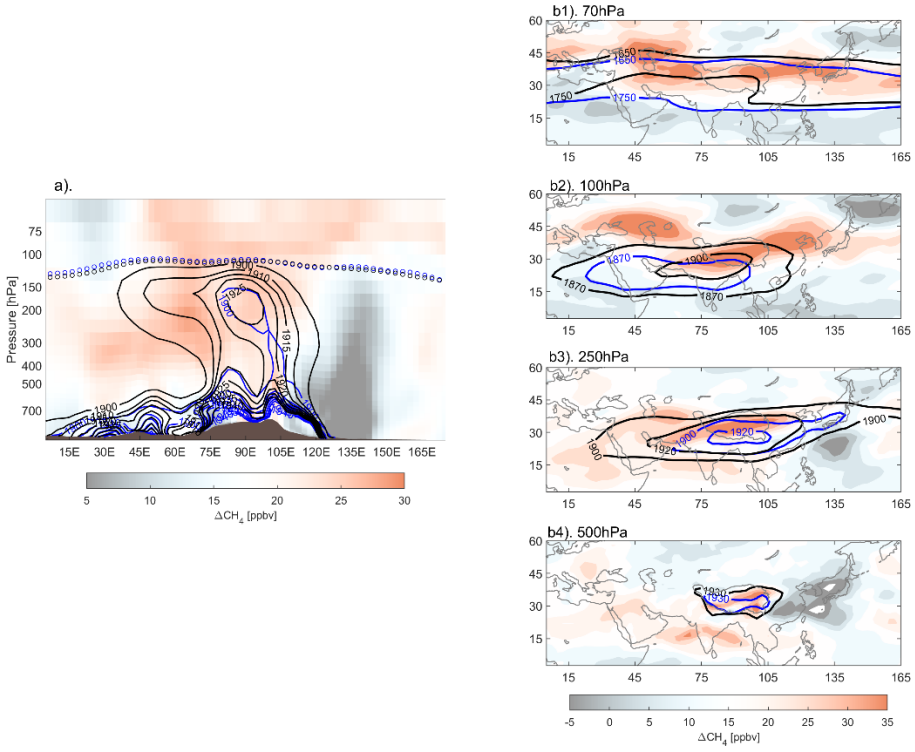

Figure 6: The seasonal (JAS) mean differences of CH_4 VMR due to anticyclone dynamics (represented by 2016LB/2018DYN minus 2016CTL). (a) Longitude-pressure cross section of CH_4 differences (averaged over 15N-40N). The horizonal distribution of CH_4 differences are shown for 70hPa (b1), 100hPa (b2), 250hPa (b3), 500hPa (b4). Contours show the methane VMR for two runs: black for 2016LB/2018DYN and blue for 2016CTL. The circles mark the tropopause for 2016 (blue) and 2018 (black).

As shown in Figure 6, changes in CH_4 concentrations driven by dynamical fields are significant in the mid-troposphere to lower stratosphere, with variations ranging from 10 to 40 ppbv. Notably, these dynamical-induced changes propagate toward the northern edge of the AMA in the UTLS. The dynamical-related methane anomalies extend northward into the lowermost stratosphere and eastward across the Pacific Ocean along the prevailing westerlies (see Figure S5).

In contrast, differences driven by emission conditions are more localized, concentrating in northern India and the Sichuan Basin within the lower troposphere (Figure 7b4), regions identified as critical for upward transport in Sec. 3.2. As the methane is transported upward into the upper troposphere, emission-related anomalies are redistributed and confined within the AMA region, as outlined by the GPH isolines (black contours) and do not significantly extend into the stratosphere.

https://doi.org/10.5194/egusphere-2024-4188
Preprint. Discussion started: 17 February 2025

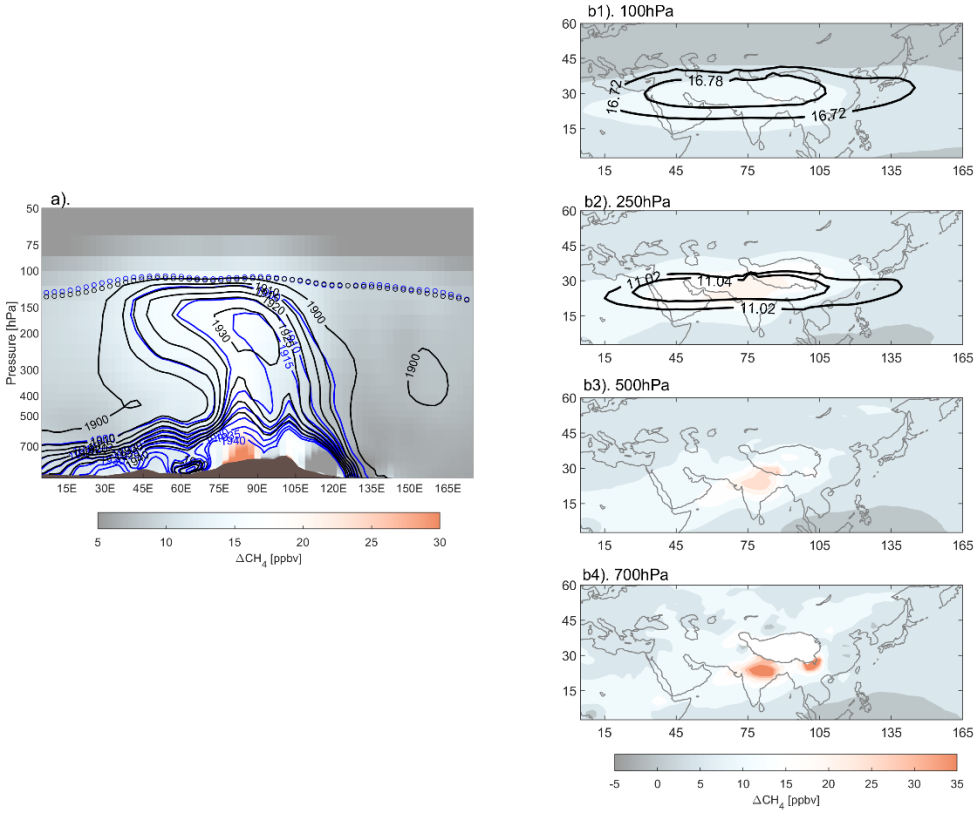

Figure 7: Similar as Figure 6 but for differences of CH_4 VMR due to emissions (represented by 2020LB/2019DYN minus 2019CTL). Contours show the methane VMR for two runs: black for 2020LB/2019DYN and blue for 2019CTL. And the black contours on (b1) &(b2) indicate the AMA (GPH contours).

4 Discussions

The model results have a reasonable representation on the CH_4 vertical and horizontal structure in comparison to the in-situ measurements and satellite datasets, which has been discussed in a previous study (Tao et al., 2024). The uncertainty in our simulation includes CH_4 emission inversion uncertainty and modelling uncertainties such as representative error (Stanevich et al., 2020, 2021), transport scheme uncertainties (Bisht et al., 2021; Saito et al., 2013) and chemistry scheme uncertainties (Murray et al., 2021; Zhao et al., 2019). Here, the *a posteriori* CH_4 fluxes used in our study show much larger interannual flux variations than the corresponding *a priori* estimates, with their uncertainties (<3%) typically 40% smaller than the *a priori* uncertainties.

Our study demonstrates two key findings: 1) the subseasonal oscillations of the Asian Monsoon Anticyclone (AMA) significantly influence the methane transport pathway and its efficiency from the lower boundary to the UTLS (upper troposphere and lower stratosphere); and 2) the interannual variations in methane enhancement in the UTLS are more strongly controlled by the conditions of AMA subseasonal oscillations than by emissions alone. Notably, regional emissions

https://doi.org/10.5194/egusphere-2024-4188
Preprint. Discussion started: 17 February 2025

and AMA conditions are not entirely independent. On one hand, monsoon-driven heavy rainfall and resulting floods can increase methane emissions, and on the other hand, the upper level divergence caused by deep convection shapes the AMA pattern. Therefore, further investigation is needed to understand the complex interactions among monsoon convection, regional emissions, and large-scale circulation, as well as how these interactions evolve under climate change.

5 Conclusions

Similar as tropospheric tracer like CO, spatial distribution of methane in the upper troposphere exhibits remarkable subseasonal variation in strong relation to the east-west oscillation of Asian Monsoon Anticyclone (AMA). Based on AMA mode composites, we confirm that the dynamic nature of the AMA, in terms of its subseasonal modes, modulates the vertical structure of CH_4 over the monsoon region. In particular, AMA centering around 80°E (WTP mode) favors the vertical transport of air from north India and Bangladesh to the upper troposphere, which contributes most significantly to the total CH_4 monsoon plume at the UT. The methane source from south China also contributes to the enhancement especially when AMA centering around 105°E (ETP mode). The vertical transport of methane is relatively weak with a horizonal redistribution at the UT when the AMA center moving around 60°E (IP mode). Quantitively, the CH_4 anomaly in the UT under WTP mode is 50%-100% higher than that under the other modes, which show enhanced connection from key source region Himalayas-Gangetic Plain to the upper-level AMA.

Our study further reveals that methane enhancement at the upper troposphere over Asian summer monsoon region is a joint effect of monsoon transport system and annual emission peak at late August mainly from rice cultivation. The monsoon dynamics consistently elevate upper tropospheric CH_4 2%~10% throughout its whole course while emissions from rice cultivation notably contribute to the CH_4 peak commonly around late August. Our model sensitivity study reveals that, as to the monsoon seasonal and regional averaged methane amplitude in the UTLS region, the influence from conditions of AMA subseasonal oscillations is more remarkable than that from conditions of emissions.

Our findings underscore the importance of monsoon dynamics and its subseasonal variability in shaping the upper tropospheric methane 3-D distribution over the Asian monsoon region. Further research is encouraged to unravel the complexities of methane transport within the monsoon system, identify the primary source regions for methane emissions, and trace the trajectory of the monsoon methane plume after the monsoon's withdrawal.

Data availability

All raw data can be provided by the corresponding authors upon request.

https://doi.org/10.5194/egusphere-2024-4188
Preprint. Discussion started: 17 February 2025

Code availability

The GEOS-Chem model of atmospheric chemistry and transport model is maintained by Harvard University (http://geos-chem.seas.harvard.edu). The ensemble Kalman filter code is publicly available at https://github.com/Rainbow1994/EnKF_CH4.git.

Author contribution

MC designed the study; SZ performed the emission inversion, forward simulation and sensitivity tests; MC analyzed the data; MT and SZ wrote the manuscript draft; All the authors reviewed and edited the manuscript.

Competing interests

The authors declare that they have no conflict of interest.

Acknowledgments

We thank the GEOS-Chem community, in particular the Harvard University team which helps maintain the GEOS-Chem model, and the NASA Global Modelling and Assimilation Office (GMAO) for providing the MERRA2 data product.

Financial support

This work was supported by the National Key R&D Program of China (no. 2022YFB3904802), by the National Natural Science Foundation of China (42105060), by the China Postdoctoral Science Foundation (E3442418), and by the Tibet Science and Technological Project (CGZH2023000385).

References

Baker, A. K., Schuck, T. J., Brenninkmeijer, C. A. M., Rauthe-Schöch, A., Slemr, F., van Velthoven, P. F. J., and Lelieveld, J.: Estimating the contribution of monsoon-related biogenic production to methane emissions from South Asia using CARIBIC observations, Geophysical Research Letters, 39, https://doi.org/10.1029/2012GL051756, 2012.

Belikov, D. A., Saitoh, N., and Patra, P. K.: An Analysis of Interhemispheric Transport Pathways Based on Three-Dimensional Methane Data by GOSAT Observations and Model Simulations, JGR Atmospheres, 127, e2021JD035688, https://doi.org/10.1029/2021JD035688, 2022.

Bergman, J. W., Fierli, F., Jensen, E. J., Honomichl, S., and Pan, L. L.: Boundary layer sources for the Asian anticyclone: Regional contributions to a vertical conduit, JGR Atmospheres, 118, 2560–2575, https://doi.org/10.1002/jgrd.50142, 2013.

https://doi.org/10.5194/egusphere-2024-4188
Preprint. Discussion started: 17 February 2025

Bisht, J. S. H., Machida, T., Chandra, N., Tsuboi, K., Patra, P. K., Umezawa, T., Niwa, Y., Sawa, Y., Morimoto, S., Nakazawa, T., Saitoh, N., and Takigawa, M.: Seasonal Variations of SF6, CO2, CH4, and N2O in the UT/LS Region due to Emissions, Transport, and Chemistry, Journal of Geophysical Research: Atmospheres, 126, e2020JD033541, https://doi.org/10.1029/2020JD033541, 2021.

Feng, L., Palmer, P., Boesch, H., and Dance, S.: Estimating surface CO2 fluxes from space-borne CO2 dry air mole fraction observations using an ensemble Kalman Filter, Atmospheric Chemistry and Physics, 9, 2619–2633, https://doi.org/10.5194/acp-9-2619-2009, 2009.

Feng, L., Palmer, P., Bosch, H., Parker, R., Webb, A., Correia, C., Deutscher, N., Domingues, L., Feist, D., Gatti, L., Gloor, M., Hase, F., Kivi, R., Liu, Y., Miller, J., Morino, I., Sussmann, R., Strong, K., Uchino, O., and Zahn, A.: Consistent regional fluxes of CH4 and CO2 inferred from GOSAT proxy XCH4 : XCO2 retrievals, 2010-2014, Atmospheric Chemistry and Physics, 17, 2017.

Garny, H. and Randel, W. J.: Dynamic variability of the Asian monsoon anticyclone observed in potential vorticity and correlations with tracer distributions, JGR Atmospheres, 118, https://doi.org/10.1002/2013JD020908, 2013.

Gelaro, R., McCarty, W., Suárez, M. J., Todling, R., Molod, A., Takacs, L., Randles, C. A., Darmenov, A., Bosilovich, M. G., Reichle, R., Wargan, K., Coy, L., Cullather, R., Draper, C., Akella, S., Buchard, V., Conaty, A., Silva, A. M. da, Gu, W., Kim, G.-K., Koster, R., Lucchesi, R., Merkova, D., Nielsen, J. E., Partyka, G., Pawson, S., Putman, W., Rienecker, M., Schubert, S. D., Sienkiewicz, M., and Zhao, B.: The Modern-Era Retrospective Analysis for Research and Applications, Version 2 (MERRA-2), https://doi.org/10.1175/JCLI-D-16-0758.1, 2017.

Krishnamurti, T. N. and Ardanuy, P.: The 10 to 20-day westward propagating mode and “Breaks in the Monsoons,” Tellus A: Dynamic Meteorology and Oceanography, 32, 15, https://doi.org/10.3402/tellusa.v32i1.10476, 1980.

Krishnamurti, T. N. and Bhalme, H. N.: Oscillations of a Monsoon System. Part I. Observational Aspects, Journal of the Atmospheric Sciences, 33, 1937–1954, https://doi.org/10.1175/1520-0469(1976)033<1937:OOAMSP>2.0.CO;2, 1976.

Lau, W. K. M., Yuan, C., and Li, Z.: Origin, Maintenance and Variability of the Asian Tropopause Aerosol Layer (ATAL): The Roles of Monsoon Dynamics, Sci Rep, 8, 3960, https://doi.org/10.1038/s41598-018-22267-z, 2018.

Luo, J., Pan, L. L., Honomichl, S. B., Bergman, J. W., Randel, W. J., Francis, G., Clerbaux, C., George, M., Liu, X., and Tian, W.: Space–time variability in UTLS chemical distribution in the Asian summer monsoon viewed by limb and nadir satellite sensors, Atmos. Chem. Phys., 18, 12511–12530, https://doi.org/10.5194/acp-18-12511-2018, 2018.

Machida, T., Matsueda, H., Sawa, Y., Niwa, Y., Tsuboi, K., Ishijima, K., Katsumata, K., Murayama, S., Morimoto, S., Goto, D., Aoki, S., and Sasakawa, M.: Atmospheric trace gas data from the CONTRAIL flask air sampling, ver.2023.1.0 (ver.2023.1.0), https://doi.org/10.17595/20230725.001, 2023.

Manney, G. L., Santee, M. L., Lawrence, Z. D., Wargan, K., and Schwartz, M. J.: A Moments View of Climatology and Variability of the Asian Summer Monsoon Anticyclone, Journal of Climate, 34, 7821–7841, https://doi.org/10.1175/JCLI-D-20-0729.1, 2021.

Murray, L., Fiore, A., Shindell, D., Naik, V., and Horowitz, L.: Large uncertainties in global hydroxyl projections tied to fate of reactive nitrogen and carbon, Proceedings of the National Academy of Sciences of the United States of America, 118, https://doi.org/10.1073/pnas.2115204118, 2021.

Nützel, M., Dameris, M., and Garny, H.: Movement, drivers and bimodality of the South Asian High, Atmospheric Chemistry and Physics, 16, 14755–14774, https://doi.org/10.5194/acp-16-14755-2016, 2016.

https://doi.org/10.5194/egusphere-2024-4188
Preprint. Discussion started: 17 February 2025

Pan, L. L., Honomichl, S. B., Kinnison, D. E., Abalos, M., Randel, W. J., Bergman, J. W., and Bian, J.: Transport of chemical tracers from the boundary layer to stratosphere associated with the dynamics of the Asian summer monsoon, JGR Atmospheres, 121, https://doi.org/10.1002/2016JD025616, 2016.

Pan, L. L., Kinnison, D., Liang, Q., Chin, M., Santee, M. L., Flemming, J., Smith, W. P., Honomichl, S. B., Bresch, J. F., Lait, L. R., Zhu, Y., Tilmes, S., Colarco, P. R., Warner, J., Vuvan, A., Clerbaux, C., Atlas, E. L., Newman, P. A., Thornberry, T., Randel, W. J., and Toon, O. B.: A Multimodel Investigation of Asian Summer Monsoon UTLS Transport Over the Western Pacific, JGR Atmospheres, 127, e2022JD037511, https://doi.org/10.1029/2022JD037511, 2022.

Park, M., Randel, W. J., Kinnison, D. E., Garcia, R. R., and Choi, W.: Seasonal variation of methane, water vapor, and nitrogen oxides near the tropopause: Satellite observations and model simulations, J. Geophys. Res., 109, 2003JD003706, https://doi.org/10.1029/2003JD003706, 2004.

Park, M., Randel, W. J., Emmons, L. K., and Livesey, N. J.: Transport pathways of carbon monoxide in the Asian summer monsoon diagnosed from Model of Ozone and Related Tracers (MOZART), J. Geophys. Res., 114, 2008JD010621, https://doi.org/10.1029/2008JD010621, 2009.

Parker, R., Webb, A., Boesch, H., Kalaitzi, N., Bergamaschi, P., Chevallier, F., Palmer, P., Feng, L., Griffith, D., Hase, F., Kivi, R., Oh, Y.-S., Ohyama, H., Pollard, D., Roehl, C., Sha, M., Shiomi, K., Strong, K., Té, Y., and Barrio Guilló, R.: A Decade of GOSAT Proxy Satellite CH4 Observations, https://doi.org/10.5194/essd-2020-114, 2020.

Ploeger, F., Konopka, P., Walker, K., and Riese, M.: Quantifying pollution transport from the Asian monsoon anticyclone into the lower stratosphere, Atmospheric Chemistry and Physics, 17, 7055–7066, https://doi.org/10.5194/acp-17-7055-2017, 2017.

Randel, W. J., Park, M., Emmons, L., Kinnison, D., Bernath, P., Walker, K. A., Boone, C., and Pumphrey, H.: Asian Monsoon Transport of Pollution to the Stratosphere, Science, 328, 611–613, https://doi.org/10.1126/science.1182274, 2010.

Riese, M., Ploeger, F., Rap, A., Vogel, B., Konopka, P., Dameris, M., and Forster, P.: Impact of uncertainties in atmospheric mixing on simulated UTLS composition and related radiative effects, J. Geophys. Res., 117, 2012JD017751, https://doi.org/10.1029/2012JD017751, 2012.

Rohs, S., Schiller, C., Riese, M., Engel, A., Schmidt, U., Wetter, T., Levin, I., Nakazawa, T., and Aoki, S.: Long-term changes of methane and hydrogen in the stratosphere in the period 1978–2003 and their impact on the abundance of stratospheric water vapor, J. Geophys. Res., 111, 2005JD006877, https://doi.org/10.1029/2005JD006877, 2006.

Rosenlof, K. H., Tuck, A. F., Kelly, K. K., Russell, J. M., and McCormick, M. P.: Hemispheric asymmetries in water vapor and inferences about transport in the lower stratosphere, J. Geophys. Res., 102, 13213–13234, https://doi.org/10.1029/97JD00873, 1997.

Saito, R., Patra, P. K., Sweeney, C., Machida, T., Krol, M., Houweling, S., Bousquet, P., Agusti-Panareda, A., Belikov, D., Bergmann, D., Bian, H., Cameron-Smith, P., Chipperfield, M. P., Fortems-Cheiney, A., Fraser, A., Gatti, L. V., Gloor, E., Hess, P., Kawa, S. R., Law, R. M., Locatelli, R., Loh, Z., Maksyutov, S., Meng, L., Miller, J. B., Palmer, P. I., Prinn, R. G., Rigby, M., and Wilson, C.: TransCom model simulations of methane: Comparison of vertical profiles with aircraft measurements, Journal of Geophysical Research: Atmospheres, 118, 3891–3904, https://doi.org/10.1002/jgrd.50380, 2013.

Schuck, T. J., Brenninkmeijer, C. A. M., Baker, A. K., Slemr, F., Von Velthoven, P. F. J., and Zahn, A.: Greenhouse gas relationships in the Indian summer monsoon plume measured by the CARIBIC passenger aircraft, Atmos. Chem. Phys., 10, 3965–3984, https://doi.org/10.5194/acp-10-3965-2010, 2010.

https://doi.org/10.5194/egusphere-2024-4188
Preprint. Discussion started: 17 February 2025

Schuldt, K. N., Aalto, T., Andrews, A., Aoki, S., Apadula, F., Arduini, J., Arlyn Andrews, Baier, B., Bartyzel, J., Bergamaschi, P., Biermann, T., Biraud, S. C., Boenisch, H., Brailsford, G., Brand, W. A., Van Der Veen, C., Chen, H., Myhre, C. L., Couret, C., Miller, C. E., Choong-Hoon Lee, Lunder, C. R., Plass-Duelmer, C., Plass-Duelmer, C., Gerbig, C., Sloop, C. D., Sweeney, C., Kubistin, D., Goto, D., Jaffe, D., Heltai, D., Lowry, D., Munro, D., Worthy, D., Dlugokencky, E., Kozlova, E., Gloor, E., Cuevas, E., Hintsa, E., Kort, E., Morgan, E., Nisbet, E., Obersteiner, F., Apadula, F., Meinhardt, F., Moore, F., Vitkova, G., Giordane A. Martins, Manca, G., Zazzeri, G., Brailsford, G., Forster, G., Santoni, G., Haeyoung Lee, Boenisch, H., Moossen, H., Timas, H., Matsueda, H., Kang, H.-Y., Huilin Chen, Lehner, I., Mammarella, I., Bartyzel, J., Elkins, J. W., Jaroslaw Necki, Pittman, J., Pichon, J. M., MÃ¼ller-Williams, J., Jgor Arduini, Turnbull, J., Miller, J. B., Lee, J., Jooil Kim, Pitt, J., DiGangi, J. P., Lavric, J., Hatakka, J., Worsey, J., Holst, J., Lehtinen, K., Kominkova, K., McKain, K., Saito, K., Davis, K., Thoning, K., TÃ¸rseth, K., Haszpra, L., SÃ¸rensen, L. L., Gatti, L. V., Emmenegger, L., Sha, M. K., Menoud, M., Delmotte, M., Fischer, M. L., De Vries, M., Schumacher, M., Torn, M., Popa, M. E., Leuenberger, M., et al.: Multi-laboratory compilation of atmospheric methane data for the period 1983-2021; obspack_ch4_1_GLOBALVIEWplus_v5.0_2022-10-17, https://doi.org/10.25925/20221001, 2022.

Siu, L. W. and Bowman, K. P.: Unsteady Vortex Behavior in the Asian Monsoon Anticyclone, Journal of the Atmospheric Sciences, 77, 4067–4088, https://doi.org/10.1175/JAS-D-19-0349.1, 2020.

Stanevich, I., Jones, D. B. A., Strong, K., Parker, R. J., Boesch, H., Wunch, D., Notholt, J., Petri, C., Warneke, T., Sussmann, R., Schneider, M., Hase, F., Kivi, R., Deutscher, N. M., Velazco, V. A., Walker, K. A., and Deng, F.: Characterizing model errors in chemical transport modeling of methane: impact of model resolution in versions v9-02 of GEOS-Chem and v35j of its adjoint model, Geoscientific Model Development, 13, 3839–3862, https://doi.org/10.5194/gmd-13-3839-2020, 2020.

Stanevich, I., Jones, D. B. A., Strong, K., Keller, M., Henze, D. K., Parker, R. J., Boesch, H., Wunch, D., Notholt, J., Petri, C., Warneke, T., Sussmann, R., Schneider, M., Hase, F., Kivi, R., Deutscher, N. M., Velazco, V. A., Walker, K. A., and Deng, F.: Characterizing model errors in chemical transport modeling of methane: using GOSAT XCH_4 data with weak-constraint four-dimensional variational data assimilation, Atmospheric Chemistry and Physics, 21, 9545–9572, https://doi.org/10.5194/acp-21-9545-2021, 2021.

Stavert, A. R., Saunois, M., Canadell, J. G., Poulter, B., Jackson, R. B., Regnier, P., Lauerwald, R., Raymond, P. A., Allen, G. H., Patra, P. K., Bergamaschi, P., Bousquet, P., Chandra, N., Ciais, P., Gustafson, A., Ishizawa, M., Ito, A., Kleinen, T., Maksyutov, S., McNorton, J., Melton, J. R., Müller, J., Niwa, Y., Peng, S., Riley, W. J., Segers, A., Tian, H., Tsuruta, A., Yin, Y., Zhang, Z., Zheng, B., and Zhuang, Q.: Regional trends and drivers of the global methane budget, Global Change Biology, 28, 182–200, https://doi.org/10.1111/gcb.15901, 2022.

Tao, M., Cai, Z., Zhu, S., Liu, Y., Feng, L., Fang, S., Yi, Y., and Bian, J.: New evidence for CH 4 enhancement at upper troposphere associated with Asian summer monsoon, Environmental Research Letters, 19, https://doi.org/10.1088/1748-9326/ad2738, 2024.

The International GEOS-Chem User Community: Geoschem/geos-chem: GEOS-Chem 12.5.0, 2019.

Tomsche, L., Pozzer, A., Ojha, N., Parchatka, U., Lelieveld, J., and Fischer, H.: Upper tropospheric CH₄ and CO affected by the South Asian summer monsoon during the Oxidation Mechanism Observations mission, Atmos. Chem. Phys., 19, 1915–1939, https://doi.org/10.5194/acp-19-1915-2019, 2019.

Total Carbon Column Observing Network (TCCON) Team: 2020 TCCON Data Release, https://doi.org/10.14291/TCCON.GGG2020, 2022.

Vogel, B., Müller, R., Günther, G., Spang, R., Hanumanthu, S., Li, D., Riese, M., and Stiller, G. P.: Lagrangian simulations of the transport of young air masses to the top of the Asian monsoon anticyclone and into the tropical pipe, Atmos. Chem. Phys., 19, 6007–6034, https://doi.org/10.5194/acp-19-6007-2019, 2019.

https://doi.org/10.5194/egusphere-2024-4188
Preprint. Discussion started: 17 February 2025

Xiong, X., Houweling, S., Wei, J., Maddy, E., Sun, F., and Barnet, C.: Methane plume over south Asia during the monsoon season: satellite observation and model simulation, Atmos. Chem. Phys., 9, 783–794, https://doi.org/10.5194/acp-9-783-2009, 2009.

Yan, X., Konopka, P., Ploeger, F., Podglajen, A., Wright, J. S., Müller, R., and Riese, M.: The efficiency of transport into the stratosphere via the Asian and North American summer monsoon circulations, Atmos. Chem. Phys., 19, 15629–15649, https://doi.org/10.5194/acp-19-15629-2019, 2019.

Yu, P., Rosenlof, K. H., Liu, S., Telg, H., Thornberry, T. D., Rollins, A. W., Portmann, R. W., Bai, Z., Ray, E. A., Duan, Y., Pan, L. L., Toon, O. B., Bian, J., and Gao, R.-S.: Efficient transport of tropospheric aerosol into the stratosphere via the Asian summer monsoon anticyclone, Proc. Natl. Acad. Sci. U.S.A., 114, 6972–6977, https://doi.org/10.1073/pnas.1701170114, 2017.

Zeng, Z.-C., Byrne, B., Gong, F.-Y., He, Z., and Lei, L.: Correlation between paddy rice growth and satellite-observed methane column abundance does not imply causation, Nat Commun, 12, 1163, https://doi.org/10.1038/s41467-021-21434-7, 2021.

Zhang, G., Xiao, X., Dong, J., Xin, F., Zhang, Y., Qin, Y., Doughty, R. B., and Moore, B.: Fingerprint of rice paddies in spatial–temporal dynamics of atmospheric methane concentration in monsoon Asia, Nat Commun, 11, 554, https://doi.org/10.1038/s41467-019-14155-5, 2020.

Zhang, Q., Wu, G., and Qian, Y.: The Bimodality of the 100 hPa South Asia High and its Relationship to the Climate Anomaly over East Asia in Summer., Journal of the Meteorological Society of Japan, 80, 733–744, https://doi.org/10.2151/jmsj.80.733, 2002.

Zhao, Y., Saunois, M., Bousquet, P., Lin, X., Berchet, A., Hegglin, M. I., Canadell, J. G., Jackson, R. B., Hauglustaine, D. A., Szopa, S., Stavert, A. R., Abraham, N. L., Archibald, A. T., Bekki, S., Deushi, M., Jöckel, P., Josse, B., Kinnison, D., Kirner, O., Marécal, V., O'Connor, F. M., Plummer, D. A., Revell, L. E., Rozanov, E., Stenke, A., Strode, S., Tilmes, S., Dlugokencky, E. J., and Zheng, B.: Inter-model comparison of global hydroxyl radical (OH) distributions and their impact on atmospheric methane over the 2000–2016 period, Atmospheric Chemistry and Physics, 19, 13701–13723, https://doi.org/10.5194/acp-19-13701-2019, 2019.

Zhu, S., Feng, L., Liu, Y., Wang, J., and Yang, D.: Decadal Methane Emission Trend Inferred from Proxy GOSAT XCH4 Retrievals: Impacts of Transport Model Spatial Resolution, Advances in Atmospheric Sciences, 39, https://doi.org/10.1007/s00376-022-1434-6, 2022.